



HAL
open science

Characterization of Surgical Tools for Specific Endovascular Navigation

Arif Badrou, Nicolas Tardif, A. Even, Philippe Chaudet, Nathan Lescanne, Jérôme Szewczyk, Anthony Gravouil, Nahiène Hamila, Aline Bel-Brunon

► **To cite this version:**

Arif Badrou, Nicolas Tardif, A. Even, Philippe Chaudet, Nathan Lescanne, et al.. Characterization of Surgical Tools for Specific Endovascular Navigation. Cardiovascular Engineering and Technology, 2022, 10.1007/s13239-022-00612-8 . hal-03676019v1

HAL Id: hal-03676019

<https://hal.science/hal-03676019v1>

Submitted on 23 May 2022 (v1), last revised 13 Jul 2022 (v2)

HAL is a multi-disciplinary open access archive for the deposit and dissemination of scientific research documents, whether they are published or not. The documents may come from teaching and research institutions in France or abroad, or from public or private research centers.

L'archive ouverte pluridisciplinaire **HAL**, est destinée au dépôt et à la diffusion de documents scientifiques de niveau recherche, publiés ou non, émanant des établissements d'enseignement et de recherche français ou étrangers, des laboratoires publics ou privés.

Characterization of surgical tools for specific endovascular navigation

A. Badrou¹, N. Tardif¹, A. Even¹, P. Chaudet¹, N. Lescanne², J. Szewczyk^{3,2}, A. Gravouil¹, N. Hamila⁴, and A. Bel-Brunon¹

¹Univ Lyon, INSA Lyon, CNRS, LaMCoS, UMR5259, 69621 Villeurbanne, France

²BaseCamp Vascular (BCV), 75005 Paris, France

³Sorbonne Université, CNRS, INSERM, Institut des Systèmes Intelligents et de Robotique, ISIR, ISIR - AGATHE, F-75005 Paris, France

⁴Ecole Nationale d'Ingénieurs de Brest, ENIB, UMR CNRS 6027, IRDL, F-29200, Brest, France

Received: date / Accepted: date

Abstract *Purpose*-The aim of this work was to mechanically characterize a specific active guidewire and catheters that are commercially available, for further implementation into numerical simulation of endovascular navigation towards complex targets.

Methods-For the guidewire, 3-point bending tests and bending with added masses were used to obtain the Young moduli of its various components. To study its behavior, the guidewire was activated under "ideal" conditions and its performance was investigated. As for the various catheters, they were measured and 3-point bending tests were conducted to determine their mechanical properties.

Results & Conclusion-The Young moduli of the shaft and the distal tip of the guidewire were determined. We defined a suitable current intensity to activate the guidewire related to an optimal curvature. Then, the time of activation / deactivation was measured at 1.7s. On the flip side, parts of the catheters were considered either elastic or viscoelastic. In all cases, the rigidity gradients along the various catheters were highlighted. The characterization of the aforementioned surgical tools provides the opportunity to simulate the endovascular navigation process.

Keywords Endovascular navigation · Guidewire · SMA · Catheter · Characterization

Introduction

Endovascular therapies have increased significantly during the past years [53] to treat various pathologies of the vascular structure. This mini-invasive surgery consists in inserting tools of increasing stiffness to navigate to the targeted area and deploy devices such as coils [15], endoprostheses [41] or balloons [40]. Navigation is a particularly crucial step that should be as efficient as possible to limit surgery time, as well as the patient's and surgeon's exposure to radiation. To reach the area to treat, different guidewires and catheters are inserted and co-manipulated. Some targets are rather *simple*, e.g. abdominal aortic aneurysms associated to a femoral access, although some difficulties may occur [13]. Others are much more *complex* because of large tortuosities or the need to cross ostia to potentially very angulated collateral arteries, e.g. renal arteries or supra-aortic trunks. Such cases, where navigation is sometimes impossible, are estimated to around 20% of the endovascular therapies [29,24,30]. In general complex navigation is limited by the available devices and the impossibility to anticipate the navigation, which therefore relies mostly on the surgeon's experience. Indeed most of the existing endovascular tools are *passive*, which means that their curvature cannot be driven by the surgeon. Only preformed guidewires and catheters are available for an improved navigation, however such devices are sometimes difficult to handle and are not suitable for all kinds of endovascular morphologies.

To improve this situation and allow more patients to benefit from endovascular therapies, new so-called *active* devices from different technologies have recently

Aline Bel-Brunon
Univ Lyon, INSA Lyon, CNRS, LaMCoS, UMR5259, 69621
Villeurbanne, France
E-mail: aline.bel-brunon@insa-lyon.fr

been proposed: Shape Memory Alloys (SMA) are often used as actuators in order to curve the devices [7, 49, 52, 2, 20, 14], while other materials like electrostrictive polymers are used to obtain a steerable guidewire [10]. They all aim to ease the navigation through tortuous arteries and enable a crossing of ostias along the path to the target.

An active device was recently proposed dedicated to complex targets such as Supra-Aortic Trunks (SATs) for interventional neuroradiology purposes. It is based on SMA [48] and is meant to be inserted first, followed by a Distal Access Catheter (DAC). The success of the navigation is therefore primarily driven by the ability of the active device and the DAC to reach the desired target. Due to its ability to bend towards large curvature, this specific active device has the potentiality to improve navigation by facilitating the hooking of SATs.

To evaluate the potential of such devices to improve the navigation, in-vitro (on phantoms), in-vivo or in-silico tests can be performed. In-silico tests based on the numerical simulation are particularly adapted to evaluate the improvement brought by a new guidewire in various cases. Numerical models can indeed simulate endovascular navigation into various anatomies, using various guidewire designs and various gestures from the clinician. Such parametric studies help defining the cases in which the active guidewire improves the clinical practice in a significant way, or cases where it is not required for a successful navigation. To build such a navigation model, accurate knowledge on the devices is required, which motivates the characterization work presented in this paper. The mechanical behaviour of the devices indeed drives their interaction with the vascular structure and the blood flow.

Different experimental tests have been used to characterize catheters or guidewires, such as tensile [38, 34] or bending [12] tests but DAC are quite particular as they comprise several portions of varying stiffness due to differing internal structures and temperature-dependant materials like polymers or Nitinol. To the best of our knowledge, no studies have been conducted to mechanically characterize endovascular active devices. As mentioned, the active guidewire of this work was based on SMAs with a thermomechanically coupled behavior [45]. Moreover, SMAs exhibit non-symmetric behavior in tension-compression [21, 1] and their mechanical properties depend on the strain rate [51, 31]. It is therefore clear that a dedicated characterization for this active guidewire is necessary.

As a first step of an endovascular navigation simulation towards complex targets using active guidewires, this paper presents a thorough characterization of the

mechanical behavior of this guidewire as well as the associated commercially available DACs.

Material & Methods

Characterization of the active guidewire

Active guidewire constitution

The active guidewire was made of a steel shaft and a tip comprising a Nitinol superelastic blade. A 30-mm Nitinol wire was attached to this blade with a spring and the assembly of the nitinol wire onto the blade defined an active modulus. The assembly (shaft and tip) was surrounded by a sheath (see Fig.1). The long shaft comprised the steel rod, the surrounding sheath and the electrical wires used to heat the active modulus which were tightly packed between the sheath and the rod. A current was applied to the active modulus enabling the Nitinol wire to be heated by Joule effect. Using the Shape Memory Effect (SME) inherent to SMA [23], the wire shrunk causing the blade to bend. SMA also exhibited Pseudoelasticity or Superelasticity [31]. The blade was therefore able to withstand large strains (up to several %) and recover its initial shape during unloading, forming a hysteresis loop.

In the following, the sheath surrounding the guidewire was always included for the characterization. Thus, characterizing the shaft would for instance consist in the characterization of the shaft and the sheath around it. The specification of the guidewire is related to the opening angle, which is the quantity of interest in this work, described by Fig.1.

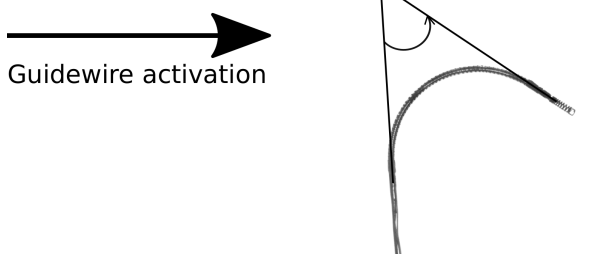
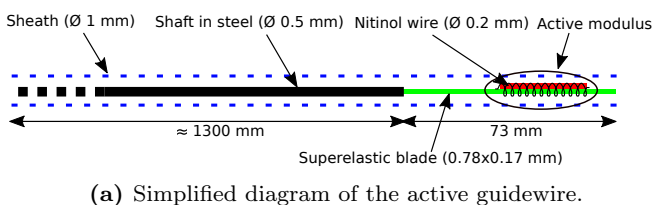


Fig. 1 Simplified diagram of the active guidewire and definition of the opening angle of the guidewire representing its performance.

The objective was to characterize the shaft, the blade and the active part. We wanted to identify the mechanical properties of the subset {shaft + sheath} and the whole {shaft + sheath + electrical wire} to get an idea of the influence of the electrical wires. Three shaft samples for each subset were available.

The two other parts that were characterized were the blade (in green) and the active modulus including several components like the Nitinol wire, the superelastic blade and a coil. Three samples were also available for both the blade and the active part.

Experimental setup for the characterization of the guidewire passive behaviour

Very few studies can be found in the literature on the characterization of endovascular devices. Except for [38] in which tensile test was used, 3-point bending test is the typical setup for guidewire and catheter mechanical characterization [35,34,12]. In this work we also use 3-point bending to characterize the guidewire shaft. However, as the guidewire distal tip is much softer than the shaft, the uncertainty would have been too large using this setup and the associated force sensor; therefore, a setup of bending under added weight was developed for the tip, inspired by studies on composite materials [27, 25,26].

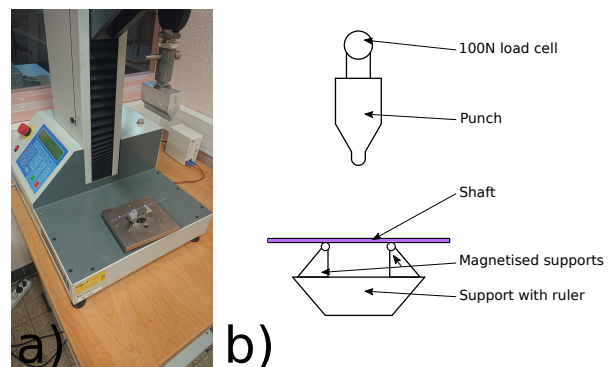


Fig. 2 Characterization of the shaft was conducted using 3-point bending method. A tensile machine Lloyd of 1kN was used in this case (a). The scheme of the 3-point bending test is presented (b).

A 3-point bending setup was used to characterise the aforementioned shaft sets (see Fig.2). It comprised two magnetized supports on a 60-mm small ruler. The gap l between the supports was fixed at 30 mm. The samples were bent by applying by three times a displacement d of 2.5 mm to the punch at 10 mm/min. Experiments regarding the active modulus and the blade

were conducted in a Binder oven (Fig.3). Prior tests were performed to study the temperature homogeneity inside the oven thanks to thermocouples. No thermal heterogeneity was found and we defined a temperature range for the oven of $[36^\circ; 37.5^\circ]$. This was expected to be our working interval considering the patients that were generally elderly and the various studies related to measuring the core temperature [36,39,28,11].

The active part and the blade underwent bending with added weight as shown in Fig.3.

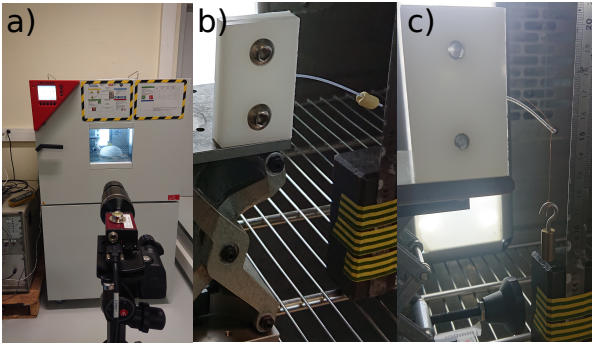


Fig. 3 Binder oven (a) and the two experimental setups used to characterize respectively the blade (b) and the active part (c).

10 mm of the sheath surrounding the studied samples was held between two plates (one of them having a thin notch). A 5-Mpx camera and a 100-mm lens were used to record the various bending shapes with the added weights. The characterization of the blade and the active part differed slightly. The steps for the blade were the following: the Binder oven was turned on, with a target temperature within the interval previously defined; the blade was held between the two plates by screws; a 10-mm and 1-g paste band was fixed at the blade tip (6 mm to the end); the blade was inserted in the oven and after 20 minutes of heating, 5 screenshots were taken as the oven fan tended to make the blade swing. These tests were performed 3 times and for various added weights (0.5g, 1.5g and 2g).

The characterisation of the blade was done at around 37°C and also at ambient temperature. The active modulus was found to be quite different as its stiffness increased: a mass of 2g was attached with a string at the tip, and no oscillations appeared so only 1 screenshot was taken. The tested masses were 2g, 5g and 10g.

Post-processing

If we denote D the rod diameter and F the force, the

Young modulus for the shaft was obtained using the beam theory:

$$E = \frac{F4l^3}{d3\pi D^4} \quad (1)$$

The entire shaft was considered elastic with the Young modulus computed and a Poisson ratio fixed at 0.3. The deformed shapes of the blade and the active part were obtained from the experimental data. We aimed to use optimization to find suitable mechanical properties. The identification was based on an inverse method called FEMU (Finite Element Method Updating). It aimed at finding the optimal set of constitutive law parameters (in this case the Young modulus) minimizing the gap between simulated and experimental data. Here, the data to minimize was the bended shape of the beam subjected to various constant loads. We started by modeling the bending tests under added masses.

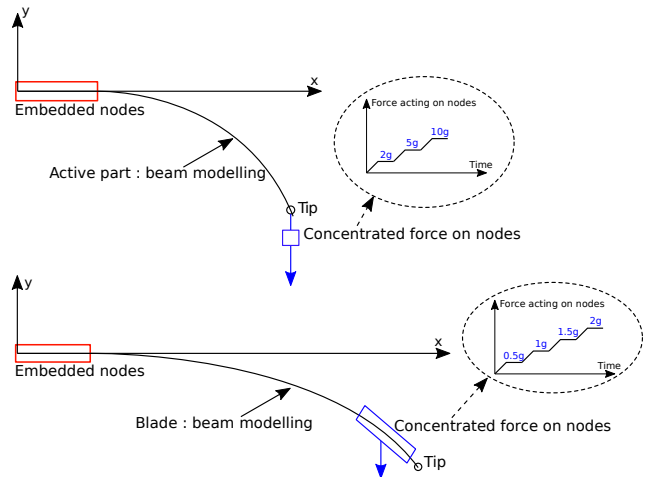


Fig. 4 Active part (top) and blade (bottom) models with step functions used to represent the added weights.

The model consisted of the blade and active part sliced into 1-mm Hughes-Liu beam elements in Ls-Dyna (Livermore Software Technology Corporation (Ansys / LST), CA., USA, 1976), a mesh size confirmed by a convergence analysis. On a number of nodes along 10 mm (paste length) for the blade and over a cubic element for the active part, we defined a step function for the concentrated force versus time. Each step was related to the various added mass and the process was simulated using an implicit method. The experimental reference coordinates of the bended beam were post-processed from the picture taken by the camera. We carried out a contour detection in MatLab (MathWorks, Inc., USA, 1984) and fitted a polynomial for each screen capture.

The number of constrained nodes was then chosen regarding the deformed shapes as slippage could occur between the sheath and the SMA component. We fixed the Poisson ratio at 0.3 for both the blade and the active part.

Once the boundary conditions were chosen, we used parameter identification in Ls-Opt (Ansys / LST, CA., USA, 1976). The input values for such a procedure were the Young moduli E_{blade} and $E_{activepart}$. The objective functions for optimization F_y and F_x were defined as:

$$\begin{cases} F_y = \sqrt{\sum_{i=1}^n W[y_{simu_i} - y_{exp_i}]^2} \\ F_x = \sqrt{\sum_{i=1}^n [x_{simu_i} - x_{exp_i}]^2} \end{cases}$$

Where y_{exp_i} and y_{simu_i} in the first equation corresponded respectively to the experimental and simulated displacements in y of the tip (last node of our model), and W was a weighting factor (2 in this case). Thus, the sum was calculated for the n displacements with respect to the different masses. We added another function F_x with a unit weighting factor taking into account the displacements in x . The optimization procedure was realized using a metamodel-based method called Successive Response Surface Method (SRSM). The metamodel was chosen to be linear and the distribution of the design points were selected by a determinant optimal (D-opt). An example of the process flow of the blade is shown Fig.5.

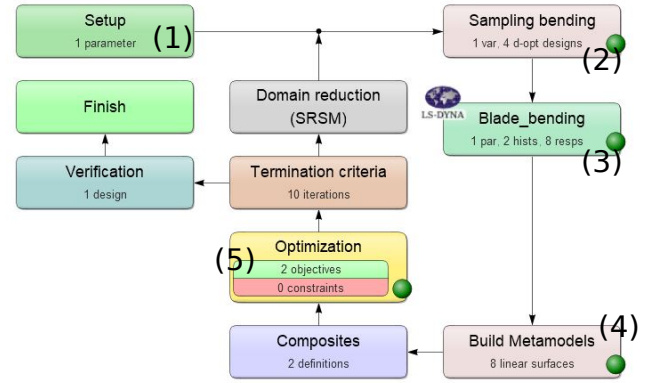


Fig. 5 Ls-Opt optimization procedure for parameter identification: example in the case of the blade. In (1) the parameter to optimize is defined, here the Young modulus of the blade. During the sampling (2) 4 values of the Young modulus are chosen in the parametric space. During the next step (3) the 8 responses, namely X and Y displacements for the 4 added mass are computed for each value of Young modulus. The metamodel was then created (4) and F_x , F_y were computed (5) for the optimization procedure.

Convergences for response accuracy, objective functions and design variables had a tolerance of 0.01. The maximum number of iterations was 10.

Guidewire controlled activation

The curvature of the guidewire depended on the electric current injected and also on the thermal influence of the surrounding fluid. The first results with one guidewire were obtained by activating it in the Binder oven (Fig.3): thanks to a current generator, we defined an appropriate current in order to have a curvature close to a target value of 50° (see the definition of opening angle in Fig.1). The goal of this part was to characterize the opening angle evolution with respect to electric current in order to have a value of the appropriate current for an opening angle close to 50° in "ideal" conditions, and to characterize the activation and deactivation time. Ideal conditions correspond to an environment mimicking blood at body temperature.

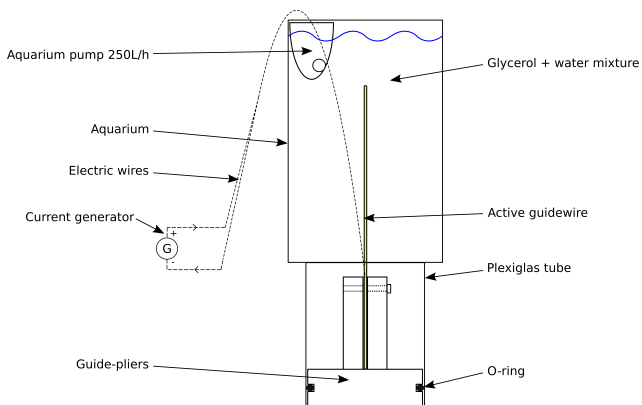


Fig. 6 Diagram of the experimental setup for the guidewire activations under "ideal" conditions.

The experimental setup consisted of "guide-pliers" holding the guidewire. A Plexiglas tube was fitted into the support with an O-ring ensuring watertightness. A rectangular aquarium was attached to the tube with putty. In the center of the aquarium there was also a hole. The activation of the guide was engaged by an electric current: electrical wires were directly connected to a current generator via crocodile clips. At the top of the aquarium a pump was placed to create a brewing of a specific mixture composed of glycerol and water in which the tested guidewire was placed. The whole setup was placed in the Binder oven for experimentation at body temperature.

This specific mixture mimicked the blood viscosity at 37°C. For large arteries under high shear rates (diameter larger than 0.5 mm), we know that the dynamic viscosity of blood, considered a Newtonian fluid, is within the range: [3.5 ; 4 Mpa.s] [5,6,46]. Moreover, blood properties in the aortic arch are more complex considering the proximity of the heart and the geometry [9]. Glycerol seemed to be appropriate in our case [37,44,18,22] and its concentration in tap water was determined using a rheometer from Anton Paar. Various concentrations were tested and the chosen one was examined three times at intervals of several days (time stability). Curves of the dynamic viscosity versus shear rates were plotted. The shear rate at the pump outlet was estimated using its velocity v_{max} and the formula:

$$\dot{\gamma} = \frac{v_{max}}{diameter_{pump}} \quad (2)$$

This way we ensured that the dynamic viscosity of our mixture was correct within a certain shear rate range. The temperature within the fluid was checked using a portable thermocouple.

The protocol for the activation experiment was the following: once the setup reached 37°C, 2 screenshots of the guidewire were taken to get the initial opening angle. Then an electric current around 0.8 A was generated and 2 screenshots were taken at every 0.02 A step. The procedure was repeated 4 times for each guidewire, with a pause of 1 min between each activation. The whole procedure was also recorded to evaluate the activation and deactivation times. The guidewire was considered as unusable above 10 activations.

Characterization of the catheters

Samples

Several commercially available catheters, usually associated with primary navigation, were investigated: an introducer Neuron Max 088 from Penumbra Inc; a DAC from Medtronic : Navien A+; two DACs from Penumbra Inc: Benchmark 071 and ACE 68.

A Distal Access Catheter is a reliable support for distal access areas towards the brain [47]. Each catheter comprised various parts having its own mechanical properties and length. These were separated by color shades. Two samples of each type were characterized.

Experimental setup

Each catheter was unrolled and both ends were attached to measure the various segments. Then, we used the 3-point bending setup previously mentioned (part shaft). Each catheter portion, defined with a color, was tested independently. Catheters are naturally slightly curved because of internal stresses so to overcome this they were straightened prior to testing and secured to the clamps with adhesive tape. Three tests of small amplitude and one of large amplitude were performed on each portion, always at 10 mm/min.

In order to elucidate the influence of the temperature on the mechanical properties, we used the Binder oven to pre-heat the devices. Since the geometries of the catheters were small, the heat losses occurred rapidly. We then decided to pre-heat the catheters at around 90°. For this they were put into an isothermal box. While one of catheter parts was subjected to 3-point bending, we inserted a thermocouple on the other side. The procedure was performed for several catheter lengths.

General post-processing procedure

Curves of "Force vs Displacement" and "Force vs Time" were obtained. There were two cases:

- For superimposed curves displaying a viscoelastic trend (hysteresis loop), the part was considered to have a viscoelastic behavior .
- For curves that did not overlap well or where the hysteresis loop was hardly discernible, the part was considered to have an elastic behavior in the absence of more accurate experimental data.

In all cases, the Young modulus E was obtained using beam theory (equation 1) in order to find a general stiffness gradient over the catheter length. We fitted the cloud from bending data points with a line computed with the least square method and passing through the origin, and then used the slope of this straight line to compute E .

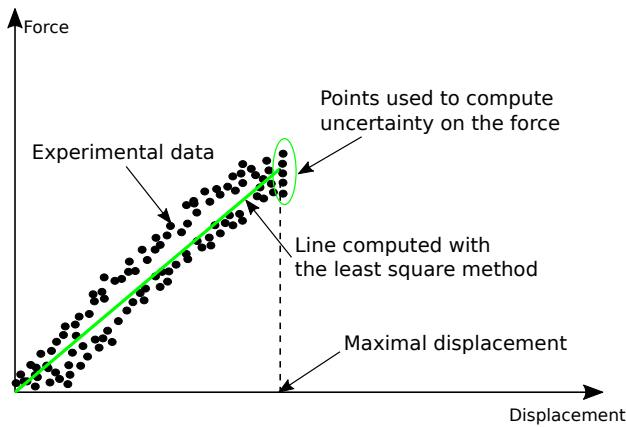


Fig. 7 Method used to idealize the experimental data where parts were considered to be elastic.

Elastic behavior

From the 3-point bending curves, we considered the part to have an elastic behavior. We followed the blue rectangles in the main diagram. From the Young modulus E obtained previously (beam theory) we modelled the 3-point bending test. The Poisson ratio ν was fixed at 0.4; an average value obtained in [38] through tensile tests on commercially available catheters.

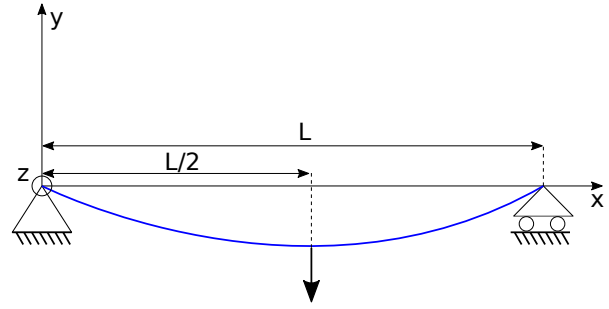


Fig. 9 Diagram of the 3-point beam modeling for elastic parts along catheters.

The catheter was modeled with beam elements in Abaqus Standard (Abaqus, Inc. (Dassault Systemes), USA, 1978). A convergence analysis concluded that the choice of 1 mm for the beam element was enough. We imposed a displacement at the center related to the one applied experimentally and extracted the reaction force F . F_{ideal} was computed using the equation of the green light in Fig.7. This force corresponded to an ideal reaction force at the center of the part considering the part as purely linear elastic. ΔF is related to uncertainty regarding the maximal force from experimental data and k is a coefficient due to the low number of samples. If F was in the defined interval, we chose the Young modulus E to be suitable for part in question.

Otherwise, we went on to refine our model by using shell elements in Abaqus. The reason for this particular choice was that segments of interest were generally too small for the use of beam elements (length of the concerned part divided by the external diameter was close to 5). The shell modeling differed from the beam one by adding representation of the supports and the punch. The element size was set to 1 mm. First of all, we used E and ν from the beam model. The output was the reaction force of the punch : we manually changed E to E^* until the reaction force was in the force range.

Viscoelastic behavior

On the basis of the experimental data, we considered some parts of the catheters as potentially viscoelastic. We were interested in the curves force versus displacement and we fitted a polynomial form to the experimental points (red curves in the following figure). We idealised once again the data with a triangle which apex was the average of the forces from bending tests. For the loading phase we computed the ratio $r_{loading} = 2 \frac{|A_{loading}|}{A_{triangle}}$ with $A_{loading}$ the difference between the area under the polynomial and the one under the green

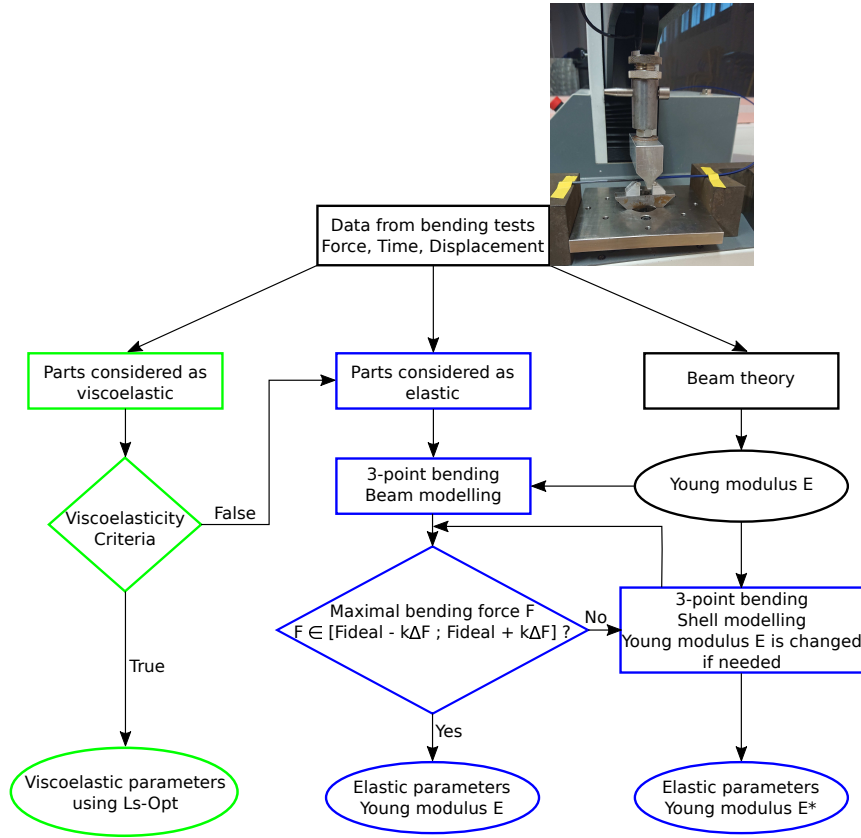


Fig. 8 Characterization procedure for the catheters from the experimental data obtained with bending tests.

triangle during loading and $A_{triangle}$ the area of the triangle. We calculated the same ratio for the unloading case:

$$r_{unloading} = 2 \frac{|A_{unloading}|}{A_{triangle}}$$

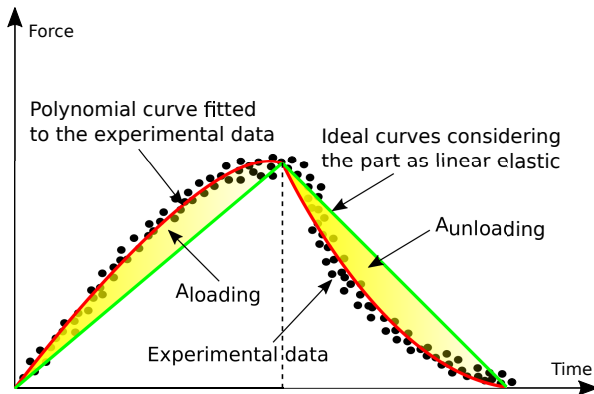


Fig. 10 Illustration of the viscoelasticity criterion highlighting the procedure used to consider a part as viscoelastic.

In order to decide if the part could be considered as viscoelastic, the ratios in percent had to respect one of the two following options:

- $r_{loading}$ and $r_{unloading}$ are greater than or equal to 20%
- $r_{loading}$ or $r_{unloading}$ is greater than or equal to 40%

These thresholds were defined arbitrarily on the basis of our experimental curves so that the chosen areas had a significant hysteresis loop. The chosen parts were modeled using a generalized Maxwell formula with one element that was composed of a spring in parallel with a dashpot and a spring in series. The shear relaxation is described by [17]:

$$G(t) = G_{\infty} + (G_0 - G_{\infty})e^{-\beta t} \quad (3)$$

G_{∞} and G_0 are respectively the long and short time shear modulus, and β is the decay constant expressed per unit of time.

The simulation was performed using Ls Dyna (with an implicit method) with Hughes-Liu beam elements of 1 mm for the catheter. Rigid shells were preferred for the supports and the punch. The catheter was partially constrained : in rotation around x and y and in

displacement along z . A displacement was applied to the upper punch. We needed to characterize the three aforementioned parameters (G_∞ , G_0 , β) and the bulk modulus B of the material. A sensitive analysis showed that B had no influence in our case, so we decided to fix this parameter using the Young modulus calculated in the previous part and the formula $B = \frac{E}{3(1-2\nu)}$.

For the remaining three parameters, we used Ls-Opt for parameter identification. The initial values were set thanks to E and ν . The ranges for optimization were defined by considering : $B > G_0 > G_\infty$. The optimization method was similar to the one used for the blade and for the active modulus characterization. The optimization problem in this section consisted in minimizing the size of the area between the experimental and simulated curves of force versus displacement.

Results

Properties of the guidewire

Shaft

The two sets {Shaft + Sheath} and {Shaft + Sheath + Electrical wires} underwent 3-point bending tests. The results are illustrated in Fig.11.

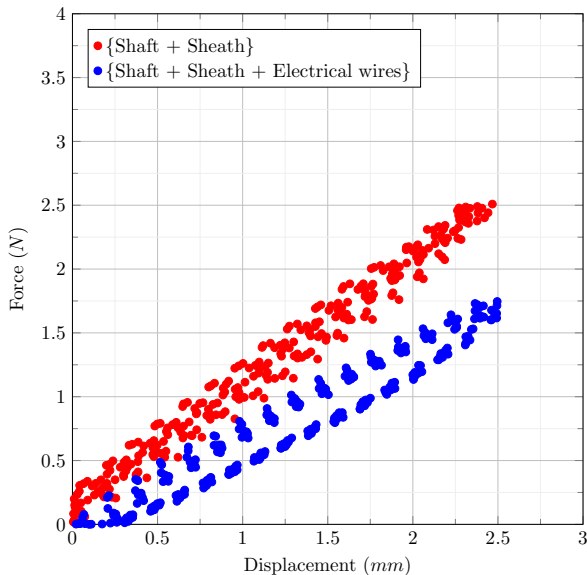


Fig. 11 Curves of force vs displacement for both {Shaft + Sheath} and {Shaft + Sheath + Electrical wires}.

With these previous experimental curves, the equation 1 and an external diameter of 1 mm, the Young

moduli were computed for the sets and are displayed in Table 1.

Table 1 Young moduli for the characterization of the shaft

	Shaft + Sheath	Shaft + Sheath + Electrical wires
Young's modulus E (MPa)	11557.7	8047.8

Table 2 Mean velocities of the clinician gestures during active navigation.

Movement	Speed values (mm/s and °/s)	Description (see Fig.5)
Pushing guidewire	21.4 ± 5.1	A
Pushing catheter	-13.5 ± 4.2	B
Pulling guidewire	12.3 ± 4.6	C
Rotating guidewire	210.9 ± 80.4	D

Mechanical properties of the guidewire's distal tip: superelastic blade and active modulus

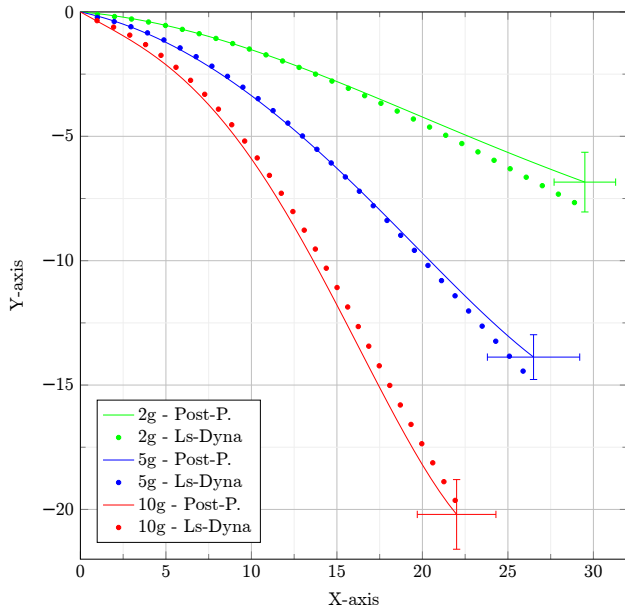
The superelastic blade and the active part underwent bending with added masses in the Binder oven. From the deformed shapes obtained, the boundary conditions (constrained nodes) were adjusted. On the flip side, we calculated the coordinates along the y (and x) axis of the tip. We proceeded to optimize in Ls-Opt and the Young moduli were computed as displayed in Table 3.

Table 3 Young moduli for the characterization of the guidewire distal tip

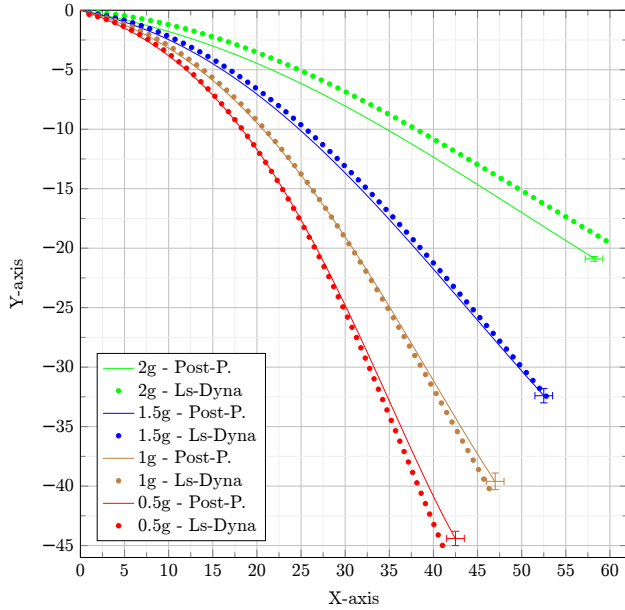
	Blade at 37°C	Blade at ambient temperature	Active part at 37°C
Young's modulus E (MPa)	52719.0	48782.1	71129.9

The difference regarding the temperature for the blade was in accordance with the literature related to the SMA: the stiffness of SMA increased with temperature [32,43,8]. The results for 37°C, experimentally shaped via post processing (Post-P.) and the coordinates of our model nodes can be seen in Fig.12 for both the blade and the active part. The results showed good agreement especially for the blade considering that its

mechanical behavior is crucial when it comes to endovascular navigation.



(a) Deformed shapes of active parts under various added weights: experimental and simulated curves (dashed lines).



(b) Deformed shapes of blades under various added weights: experimental and simulated curves (dashed lines).

Fig. 12 Comparison between experimental curves and simulated ones after parameter identification. The Y-axis is the vertical axis oriented in the direction opposite to gravity.

Guidewire activation under "ideal" conditions

The first step for aforementioned setup was to find a

suitable mixture to approach the blood viscosity. Several concentrations were tested and a mixture of 47% of glycerol in tap water was an appropriate choice with a mean dynamic viscosity of 3.8 MPa.s. The results for the 5 guidewire activations per device are shown in the following figure.

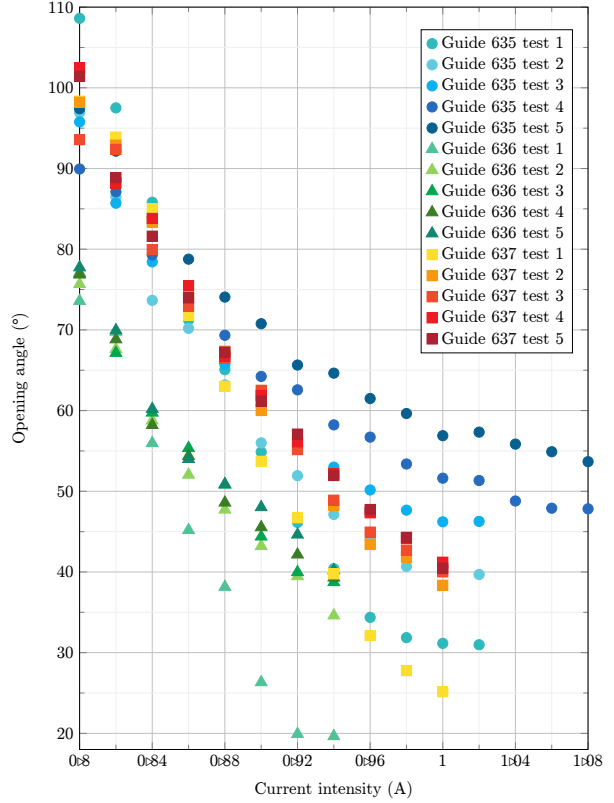


Fig. 13 Curves of opening angle vs current intensity for the 3 active guidewires tested in "ideal" conditions.

It can be noticed that the first activation was often distant from the other data. The activations tended to stabilize as the current intensity increased but there were some noticeable differences from one guide to another. The guidewires were made manually. Thus, the results were rather satisfying and the repeatability problem became relative. The current intensity of 0.92 A was the best candidate in order to get a curvature close to 50°.

Besides, the successive filmed activations of the guide made it possible to conclude that (1) the activation and deactivation times were similar, and (2) the mean time of 1.70s for the activation / deactivation was measured.

In order to simulate the activation of the guidewire, a 1D user material law was implemented in Ls-Dyna to represent the Shape Memory Effect based on the Tanaka model [50, 19]. If we denote σ the stress, E the

Young modulus, ϵ_L the recoverable maximum strain, ϵ the strain and ξ the volume fraction of SMA; the constitutive equation can be written:

$$\dot{\sigma} = E(\xi)\dot{\epsilon} - \epsilon_L E(\xi)\dot{\xi} \quad (4)$$

ξ is a function of σ and the temperature. Its expression changes depending on the direction of the transformation (cooling or heating). Tensile tests on the Nitinol wire were conducted to obtain the main properties of our law. Then, a sensitive analysis showed that only one parameter was decisive regarding the guide curvature: the recoverable maximum strain ϵ_L . This previous parameter was fixed to obtain an opening angle of 50° . The guide activation was driven by temperature. Thus, the curve temperature in our model was scaled as the activation / deactivation time was close to the 1.70s obtained experimentally.

Catheters identification

Measurements

Firstly, the various portions of the catheters were identified and measured. We can notice the particular tip of some catheters : a so-called multi-purpose tip oriented at 25° .

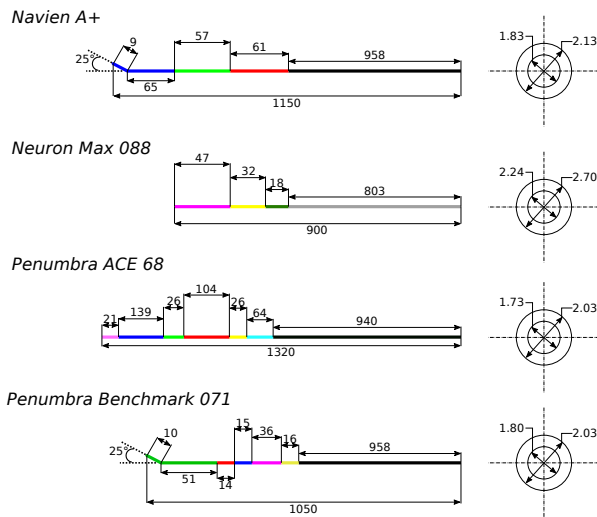


Fig. 14 Measurements of various parts for the different catheters (in mm).

Mechanical properties

All the mechanical parameters for both the viscoelastic and elastic parts are given in Tab.4 for the 4 catheters.

Figures 1 to 7 are related to the catheter part from the distal tip to the proximal one. A stiffness gradient was indeed highlighted along each device. In [38,12], mechanical characterizations of catheters used for abdominal aneurysm treatments were conducted. Values of Young modulus for the distal tip between 50 to 400 MPa were found. A stiffness gradient was also determined and the Young modulus for the most proximal parts of the catheters ranged from 300 to 2000 MPa. In [54] a value of 380 MPa was used to represent the rigidity of the distal tip of a particular spherical-tip catheter dedicated to coronary artery stenosis. These catheters deal with navigation in areas close to the aortic arch. The values of Young modulus obtained in our study for the distal and proximal parts of the different catheters are of the same order of magnitude compared to the literature, which is consistent.

Discussion

Major results

An active guidewire and commercially available catheters were mechanically characterized as part of an endovascular navigation device. Gaining insight into their mechanical behavior is required for further navigation simulations.

Assumptions about the active guidewire

We made the assumption of an elastic behavior for the distal tip of the active guidewire including the super-elastic blade and the active part. Regarding the blade, we assumed from the literature that threshold stresses were generally high enough to consider the blade as elastic during the endovascular navigation [33,16,43]. Even if we simulated the guidewire activation, which is in fact the opportune case for high stresses, we can not ensure that the blade would always behave elastically: the Nitinol grade used for the blade (and also for the active part) may be lower than those found in the literature and abrupt gestures by the clinicians could occur during the surgical treatment leading to an inelastic behaviour.

The same comments are valid for the active part, which was composed of at least a Nitinol wire, a sheath, the aforementioned blade, glue and a coil in stainless steel or Nitinol. When subjected to large strains, this complex assembly probably has a non-linear behavior. However, taking into account its small length (generally around 40 mm) and considering that the active modulus undergoes few strains during passive navigation, the hypothesis of elasticity seems reasonable.

Table 4 Mechanical properties along the four studied catheters from the distal part numbered 1 to the proximal one numbered 4, 6 or 7 depending on the catheter model.

	1	2	3	4	5	6	7
Navien	$\beta = 0.22 \text{ s}^{-1}$ $G_0 = 62.0 \text{ MPa}$ $G_{inf} = 15.9 \text{ MPa}$ $B = 82.9 \text{ MPa}$	$\beta = 0.16 \text{ s}^{-1}$ $G_0 = 94.1 \text{ MPa}$ $G_{inf} = 26.6 \text{ MPa}$ $B = 152.3 \text{ MPa}$	$\beta = 0.18 \text{ s}^{-1}$ $G_0 = 448.1 \text{ MPa}$ $G_{inf} = 152.2 \text{ MPa}$ $B = 694.6 \text{ MPa}$	$E = 1519 \text{ MPa}$			
Neuron	$\beta = 0.26 \text{ s}^{-1}$ $G_0 = 74.0 \text{ MPa}$ $G_{inf} = 17.0 \text{ MPa}$ $B = 122.1 \text{ MPa}$	$E = 250 \text{ MPa}$	$E = 180 \text{ MPa}$	$E = 1701 \text{ MPa}$			
Benchmark	$E = 124 \text{ MPa}$	$E = 150 \text{ MPa}$	$E = 189 \text{ MPa}$	$E = 493 \text{ MPa}$	$E = 570 \text{ MPa}$	$E = 3994 \text{ MPa}$	
Ace	$\beta = 0.20 \text{ s}^{-1}$ $G_0 = 15 \text{ MPa}$ $G_{inf} = 3.3 \text{ MPa}$ $B = 26.3 \text{ MPa}$	$\beta = 0.21 \text{ s}^{-1}$ $G_0 = 53.7 \text{ MPa}$ $G_{inf} = 15.2 \text{ MPa}$ $B = 106.1 \text{ MPa}$	$E = 91 \text{ MPa}$	$E = 191 \text{ MPa}$	$E = 331 \text{ MPa}$	$E = 745 \text{ MPa}$	$E = 3268 \text{ MPa}$

Another effect related to SMA is a localization phenomenon that could appear, referring to Lüders band pattern in low carbon steels [4, 3]. However, one could suppose that during endovascular navigation the active module and the superleastic blade are subjected to strains almost instantly. Besides, given the geometries (thin thickness) of these two parts, the localization phenomenon is minimized.

Study limitations for the guidewire activation

Regarding the activation of the guidewire under "ideal" conditions, some limitations affected the results and we could consider that the uncertainty when measuring the opening angle was within a range of $\pm 5^\circ$. In order to study the behavior of the active guide in detail, a larger number of samples should be considered. Then, the conditions of the study were quite far from the physiological ones as we did not represent the real pulsed blood flow. However, navigation into phantoms and in animals have shown that the guidewire is affected by the blood flow in a very limited way.

Catheter identification

The catheters were characterized using 3-point flexural tests at ambient temperature and in the open air. However, they usually have a hydrophilic coating and are composed of temperature-dependent components; features that may affect their mechanical response. Moreover, the catheters were rather fragile, and could be damaged during testing. We thus assume that repeating the tests several times and on two catheters helped overcome this limitation.

Catheters: influence of temperature

The first results related to the catheters were obtained at ambient temperature (around 20°C). We aimed at

studying the influence of temperature considering that the mechanical properties (especially for the viscoelastic parts) of the catheters are temperature-dependent. Several parts of the Navien A+ and the Neuron Max were subjected to 3-point flexural tests and the highest temperature we had was 28°C because of heat losses. At this temperature, the curves were quite similar to those obtained at ambient temperature. We can assume that the difference related to the properties between 28°C and 37°C were likely the same.

Conclusion

Surgical devices were characterized in the framework of a numerical project consisting in the development of a tool for clinicians supporting decision-making. Several methods from the literature helped us to deal with the particularities of the SMA and thin geometries: an experimental setup for bending under added weights made it possible to identify the Young moduli of the distal tip of the guidewire (blade and active part). Thanks to a more classical 3-point bending test, the shaft and the catheters were identified. In addition, we tried to refine the characterization of the catheters by adding a viscoelastic behavior owing to a complex assembly of polymers and SMA. An original setup finally helped us to understand the guidewire behavior by activating it in "ideal" conditions. Future work is threefold: first, additional characterization could be performed on the devices. Activating the guidewire in a more realistic blood flow (higher speed, higher pressure) could provide more insight in the thermal exchanges between blood and guidewire, to know whether blood flow alters the SMA activation. Besides, characterizing the DACs in an oven at 37°C could lead to adjusting the identified elastic and viscoelastic parameters to more realistic values. Second the experimental data collected on the guidewire activation will be used to identify the parameters of a SMA material model, to be further im-

plemented into a guidewire numerical model. Finally, the constitutive laws identified for the guidewire and DACs will be implemented into a numerical model of endovascular navigation. The simulation could provide design guidelines for the active guidewire depending on the patient anatomy and location of the target.

Declarations

Funding

The French National Research Agency (ANR) partially supported this work through the DEEP project: Devices for augmented Endovascular navigation in complex Pathways (grant n°ANR-18-CE19-0027-01).

Conflicts of interest

The authors declare that there are no conflicts of interest.

Availability of data and material

Not applicable

Code availability

Not applicable

References

1. R. R. Adharapurapu, F. Jiang, K. S. Vecchio, and G. T. Gray. Response of NiTi shape memory alloy at high strain rate: A systematic investigation of temperature effects on tension-compression asymmetry. *Acta Mater.*, 54(17):4609–4620, 2006.
2. A. Ali, T. Szili-Torok, M. Stijnen, P. Breedveld, and D. Dodou. First Expert Evaluation of a New Steerable Catheter in an Isolated Beating Heart. *Cardiovasc Eng Technol*, 11(6):769–782, Dec. 2020. Edition: 2020/11/18 Publisher: Springer International Publishing.
3. V. S. Ananthan and E. O. Hall. Macroscopic aspects of Lüders band deformation in mild steel. *Acta Metallurgica et Materialia*, 39(12):3153–3160, 1991.
4. N. J. Bechle and S. Kyriakides. Localization in NiTi tubes under bending. *Int. J. Solids Struct.*, 51(5):967–980, 2014.
5. N. Benard, R. Perrault, and D. Coisne. Blood flow in coronary artery: numerical fluid dynamics analysis. *Conf Proc IEEE Eng Med Biol Soc*, 5:3800–3, 2004.
6. Y. Cho and K. Kensey. Effects of the non-Newtonian viscosity of blood on flows in a diseased arterial vessel. Part 1: Steady flows. *Biorheology*, 28:241–62, 1991.
7. T. Couture and J. Szewczyk. Design and Experimental Validation of an Active Catheter for Endovascular Navigation. *J. Med. Devices*, 12(011003), Nov. 2017.
8. T. Duerig, A. Pelton, and K. Bhattacharya. The Measurement and Interpretation of Transformation Temperatures in Nitinol. *Shape Memory and Superelasticity*, 3, 2017.
9. Y. C. Fung. *Biomechanics: Motion, Flow, Stress, and Growth*. Springer-verlag new york edition, 1990.
10. F. Ganet, M. Q. Le, J. F. Capsal, P. Lermusiaux, L. Petit, A. Millon, and P. J. Cottinet. Development of a smart guide wire using an electrostrictive polymer: option for steerable orientation and force feedback. *Scientific Reports*, 5(1):18593, Dec. 2015.
11. I. I. Geneva, B. Cuzzo, T. Fazili, and W. Javaid. Normal Body Temperature: A Systematic Review. *Open Forum Infect Dis*, 6(4):ofz032–ofz032, Apr. 2019. Publisher: Oxford University Press.
12. J. Gindre, A. Bel-Brunon, M. Rochette, A. Lucas, A. Kaladji, P. Haignon, and A. Combescure. Patient-Specific Finite-Element Simulation of the Insertion of Guidewire During an EVAR Procedure: Guidewire Position Prediction Validation on 28 Cases. *IEEE. Trans. Biomed. Eng.*, 64:1–1, 2016.
13. S. S. Goyal, M. M. Panditrao, and A. Garg. The accidental loss of guidewire during emergency femoral central venous cannulation: A case report. *Adesh University Journal of Medical Sciences & Research*, 2.
14. Y. Haga, Y. Tanahashi, and M. Esashi. Small diameter active catheter using shape memory alloy. In *Proceedings MEMS 98. IEEE. Eleventh Annual International Workshop on Micro Electro Mechanical Systems. An Investigation of Micro Structures, Sensors, Actuators, Machines and Systems (Cat. No.98CH36176*, pages 419–424, Jan. 1998. ISSN: 1084-6999.
15. K. Harada and J. Morioka. Initial experience with an extremely soft bare platinum coil, ED coil-10 Extra Soft, for endovascular treatment of cerebral aneurysms. *J. Neurointerv. Surg.*, 5, 2012.
16. E. Henderson, D. H. Nash, and W. M. Dempster. On the experimental testing of fine Nitinol wires for medical devices. *J. Mech. Behav. Biomed. Mater.*, 4(3):261–268, 2011.
17. L. R. Herrmann and F. E. Peterson. A Numerical Procedure for Viscoelastic Stress Analysis. Orlando, FL., 1968.
18. P. R. Hoskins, T. Loupas, and W. N. McDicken. A comparison of the doppler spectra from human blood and artificial blood used in a flow phantom. *Ultrasound Med. Biol.*, 16(2):141–147, 1990.
19. L. Ianucci, P. Robinson, and W. Wan A Hamid. The Development of a User Defined Material Model for NiTi SMA Wires, 2017.
20. J. Jayender, R. V. Patel, and S. Nikumb. Robot-assisted Active Catheter Insertion: Algorithms and Experiments. *Int. J. Robot. Res*, 28(9):1101–1117, 2009. eprint: <https://doi.org/10.1177/0278364909103785>.
21. D. Jiang, C. M. Landis, and S. Kyriakides. Effects of tension/compression asymmetry on the buckling and recovery of NiTi tubes under axial compression. *Int. J. Solids Struct.*, 100-101:41–53, 2016.
22. S. Kim, B. Prasad, and J. Kim. Alignment of Microbeads Using Spinning Helical Minichannel Cartridge. *Journal of the Korean Society of Visualization*, 14:38–45, 2016.
23. D. C. Lagoudas. *Shape Memory Alloys*. Springer, Boston, MA, 2008.
24. R. C. Lam, S. C. Lin, B. DeRubertis, R. Hyneczek, K. C. Kent, and P. L. Faries. The impact of increasing age on

- anatomic factors affecting carotid angioplasty and stenting. *J. Vasc. Surg.*, 45(5):875–880, May 2007. Publisher: Elsevier.
25. B. Liang, P. Chaudet, and P. Boisse. Curvature determination in the bending test of continuous fibre reinforcements: Curvature Determination in the Bending of Fibre Reinforcements. *Strain*, 53, 2016.
 26. B. Liang, J. Colmars, and P. Boisse. A shell formulation for fibrous reinforcement forming simulations. *Part A Appl. Sci. Manuf.*, 100:81–96, 2017.
 27. B. Liang, N. Hamila, M. Peillon, and P. Boisse. Analysis of thermoplastic prepreg bending stiffness during manufacturing and of its influence on wrinkling simulations. *Part A Appl. Sci. Manuf.*, 67:111–122, 2014.
 28. S.-H. Lu and Y.-T. Dai. Normal body temperature and the effects of age, sex, ambient temperature and body mass index on normal oral temperature: A prospective, comparative study. *Int. J. Nurs. Stud.*, 46(5):661–668, 2009.
 29. S. Macdonald, R. Lee, R. Williams, and G. Stansby. Towards Safer Carotid Artery Stenting. *Stroke*, 40(5):1698–1703, 2009.
 30. S. Madhwal, V. Rajagopal, D. Bhatt, C. Bajzer, P. Whitlow, and S. Kapadia. Predictors of Difficult Carotid Stenting as Determined by Aortic Arch Angiography. *J. Invasive. Cardiol.*, 20:200–4, 2008.
 31. A. Maynadier, D. Depriester, K. Lavernhe-Taillard, and O. Hubert. Thermo-mechanical description of phase transformation in Ni-Ti Shape Memory Alloy. *Procedia Eng.*, 10:2208–2213, 2011.
 32. A. McKelvey and R. Ritchie. Fatigue-crack propagation in Nitinol, a shape-memory and superelastic endovascular stent material. *J. Biomed. Mater. Res.*, 47:301–8, 2000.
 33. A. L. McKelvey and R. O. Ritchie. Fatigue-crack growth behavior in the superelastic and shape-memory alloy nitinol. *Metallurgical and Materials Transactions A*, 32(13):731–743, Mar. 2001.
 34. M. Menut. *Chirurgie endovasculaire virtuelle pour patient-spécifique : Application au traitement de l'anévrisme de l'aorte thoracique*. PhD Thesis, 2017.
 35. H. Mohammadi, S. Lessard, E. Therasse, R. Mongrain, and G. Soulez. A Numerical Preoperative Planning Model to Predict Arterial Deformations in Endovascular Aortic Aneurysm Repair. *Annals of Biomedical Engineering*, 46(12):2148–2161, Dec. 2018.
 36. D. S. Moran and L. Mendal. Core Temperature Measurement. *Sports Medicine*, 32(14):879–885, Dec. 2002.
 37. A. Moravia, W. Pan, H. W. Berre, M. Menut, B. B. Said, M. E. Hajem, X. Escriva, P. Kulisa, S. Simoëns, P. Lermusiaux, A. Millon, and I. Naudin. IN VITRO ASSESSMENT OF ABDOMINAL AORTA NON-NEWTONIAN HEMODYNAMICS BASED ON PARTICLE IMAGE VELOCIMETRY. 2019.
 38. G. Mouktadiri, B. Bou-Saïd, and H. Walter-Le-Berre. Aortic endovascular repair modeling using the finite element method. *J. Biomed. Eng*, 2013.
 39. I. Pušnik and A. Miklavec. Dilemmas in Measurement of Human Body Temperature. *Instrum. Sci. Tech.*, 37(5):516–530, 2009. Publisher: Taylor & Francis _eprint: <https://doi.org/10.1080/10739140903149061>.
 40. Z. Qasim, M. Brenner, J. Menaker, and T. Scalea. Resuscitative endovascular balloon occlusion of the aorta. *Resuscitation*, 96:275–279, Nov. 2015. Publisher: Elsevier.
 41. R. Rhee, B. Peterson, E. Moore, M. Lepore, and G. Oderich. Initial human experience with the GORE EXCLUDER Conformable AAA Endoprosthesis. *J. Vasc. Surg. Cases Innov. Tech.*, 5:319–322, 2019.
 42. D. Roy, G. Holzapfel, C. Kauffmann, and G. Soulez. Finite element analysis of abdominal aortic aneurysms: geometrical and structural reconstruction with application of an anisotropic material model. *IMA J. Appl. Math.*, 79:1011–1026, 2014.
 43. A. Runciman, D. Xu, A. R. Pelton, and R. O. Ritchie. An equivalent strain/Coffin–Manson approach to multiaxial fatigue and life prediction in superelastic Nitinol medical devices. *Biomaterials*, 32(22):4987–4993, 2011.
 44. J. B. Segur and H. E. Oberstar. Viscosity of Glycerol and Its Aqueous Solutions. *Ind. Eng. Chem.*, 43(9):2117–2120, Sept. 1951. Publisher: American Chemical Society.
 45. J. A. Shaw and S. Kyriakides. Thermomechanical aspects of NiTi. *J. Mech. Phys. Solids*, 43(8):1243–1281, 1995.
 46. T. Sochi. Non-Newtonian Rheology in Blood Circulation. 2013.
 47. A. M. Spiotta, M. S. Hussain, T. Sivapatham, M. Bain, R. Gupta, S. I. Moskowitz, and F. K. Hui. The Versatile Distal Access Catheter: The Cleveland Clinic Experience. *Neurosurgery*, 68(6):1677–1686, 2011. _eprint: <https://academic.oup.com/neurosurgery/article-pdf/68/6/1677/32587534/00006123-201106000-00031.pdf>.
 48. J. Szewczyk. Process for Manufacturing a Flexible Elongate Structure Having an Orientable End, Sept. 2011.
 49. J. Szewczyk, E. Marchandise, P. Flaud, L. Royon, and R. Blanc. Active Catheters for Neuroradiology. *J. Robotics Mechatronics*, 23:105–115, 2011.
 50. K. Tanaka, S. Kobayashi, and Y. Sato. Thermomechanics of transformation pseudoelasticity and shape memory effect in alloys. *Int. J. Plast*, 2(1):59–72, 1986.
 51. H. Tobushi, Y. Shimeno, T. Hachisuka, and K. Tanaka. Influence of strain rate on superelastic properties of TiNi shape memory alloy. *Mech. Mater.*, 30(2):141–150, 1998.
 52. C. M. Wayman and T. W. Duerig. An Introduction to Martensite and Shape Memory. In T. W. Duerig, K. N. Melton, D. Stöckel, and C. M. Wayman, editors, *Engineering Aspects of Shape Memory Alloys*, pages 3–20. Butterworth-Heinemann, 1990.
 53. M. Wilbring, M. Rehm, T. Ghazy, M. Amler, K. Matschke, and U. Kappert. Aortic Arch Mapping by Computed Tomography for Actual Anatomic Studies in Times of Emerging Endovascular Therapies. *Ann. Vasc. Surg.*, 30, 2015.
 54. L. Qi, W. Zhu, W. Qian, L. Xu, Y. He, and F. Zhao. The Performance of a Spherical-tip Catheter for Stent Post-dilation: Finite Element Analysis and Experiments. *Frontiers in Physiology*, 12:1305, 2021.